PROF. AIRODY VASUDEVA ADHIKARI (Orcid ID : 0000-0002-0141-4454)

Article type : Research Article

Simple 3,6-disubstituted Carbazoles as Potential Hole-Transport Materials: Photophysical, Electrochemical and Theoretical Studies

Kavya S. Keremane [a], Rathnamala Rao [b], and Airody Vasudeva Adhikari [a,c,*]

[a] Organic Materials Laboratory, Department of Chemistry, National Institute of Technology Karnataka, Surathkal, Mangalore-575025, India

[b] Department of Electronics and Communication Engineering, National Institute of Technology Karnataka, Surathkal, Mangalore-575025, India

[c] Yenepoya Research Centre, Yenepoya deemed to be University, Deralakatte, Mangalore-575 018, India

*Corresponding author e-mail: *avachem@gmail.com ; avachem@yenepoya.edu.in* (A. Vasudeva Adhikari)

This article has been accepted for publication and undergone full peer review but has not been through the copyediting, typesetting, pagination and proofreading process, which may lead to differences between this version and the Version of Record. Please cite this article as doi: 10.1111/PHP.13337

ABSTRACT

Developing effective and low-cost organic hole-transporting materials (HTMs) is crucial for the construction of high-performance perovskite solar cells (PSCs) and to promote their production in commercial ventures. In this context, we herein report the molecular design, synthesis, and characterization of two novel D-A-D-A-D architectured 9-(2-ethylhexyl)-9*H*-carbazoles, connecting the mono/dimethoxy phenyl substituted cyanovinylene side arms symmetrically at 3rd and 6th positions of the carbazole heterocycle (**CZ$_{1-2}$**), as potential hole-

transporting materials (HTMs). The current work highlights their structural, photophysical, thermal, electrochemical, and theoretical investigations, including their structure-property correlation studies. Evidently, the optical studies showcased their excellent fluorescence ability due to their push-pull natured structure with extended π-conjugation. Further, in-depth solvatochromic studies demonstrated their intramolecular charge-transfer (ICT) dominated optoelectronic behavior, supported by various correlation studies. Also, the optical results revealed that **CZ$_1$** and **CZ$_2$** display λ_{abs} and λ_{emi} in the order of 410-430 nm and 530-560 nm, *respectively*, with a bandgap in the range of 2.5-2.6 eV. Finally, their quantum chemical simulations have provided an insight into the predictions of their structural, molecular, electronic, and optical parameters. Conclusively, the study furnishes a deeper understanding of the intricacies involved in the structural modification of carbazole-based HTMs for achieving better performance.

Keywords: Hole-transport materials; donor-acceptor; carbazoles; electrooptical properties; low-cost; density functional theory

INTRODUCTION

Designing new organic molecules as efficient charge extraction as well as transport materials in the optoelectronic based devices remains a great challenge for many photovoltaic technologies like electrophotographic photoreceptors, photovoltaics (OPVs), organic light-emitting diodes (OLEDs), and photorefractive components.[1–4] In fact, HTM is considered as an important active component in perovskite solar cells (PSCs), which is highly responsible for

efficient photogenerated hole extraction mainly at the perovskite/HTM interface and avoiding unwanted charge transfer processes, thereby bringing about an enhanced device-performance.[5,6] Generally, the device architecture of PSCs comprises a light-absorbing (perovskite) layer sandwiched between an electron transport material (ETM) and an HTM. The device may be of the type either *p-i-n* or *n-i-p* planar hybrid structure.[7] To achieve a high device-efficiency, their well-aligned energy levels with perovskite are critical: HOMO energy level must be less negative than that of perovskite material for efficient hole injection, whereas the high-lying LUMO energy level would ensure low electron affinity enabling sufficient electron blocking characteristics.[8,9] An ideal hole-transporting material must possess enhanced hole mobility to minimize losses during hole transport to the contact, as well as superior conductivity.[10] Further, it must be easily soluble and it should not require strong polar solvents for dissolution, since such solvents may dissolve the perovskite material of the cell also.[11] Furthermore, as perovskite is very sensitive to humidity and atmospheric oxygen attack, the HTM layer should function as protection from the moist air and inhibit the diffusion of external species.[12] So, very high thermal and photochemical stability, as well as superior hydrophobicity, are desirable characteristics of HTM to resist degradation factors and ensure long-standing durability. On the other hand, for ensuring the low-cost of PSC production, an ideal HTM is to be easily affordable for a reasonable cost.[13, 14]

Consequently, a vast research interest has raised for the development of new organic HTMs and also to investigate a better understanding of the correlation between the HTM and the performance of PSC.[15] A significant number of organic HTMs have been introduced so far, to achieve the requirements of an ideal candidate. The most commonly used up-to-date organic HTMs, *viz.* 2,2',7,7'-tetrakis[*N,N*-di-(*p*-methoxyphenyl)amino]-9,9'-spirobifluorene (Spiro-OMeTAD) and even further interesting macromolecule poly[bis(*p*-phenyl)2,4,6-trimethylphenyl)amine] (PTTA) were shown to deliver the PCE of >20% in the device.[1,16] However, their limitations such as tedious multi-step synthesis, complicated purification steps, instability to humid air, and difficulty in controlling conductivity, stimulate further research to investigate more cost-effective, stable, and dopant-free materials for easy commercialization.[17] In this respect, many efforts have been devoted to exploring better alternatives to the existing materials like spiro-OMeTAD.[18,19]

Recently, organic small molecules like branched methoxy diphenylamine substituted fluorene derivatives were shown to yield the power conversion efficiency (*PCE*) up to 20%, but

their synthetic methods are expensive.[20] Moreover, they need dopants like lithium salt of bis(trifluoromethylsulfonyl)imide (LiTFSI) and 4-*tert*-butylpyridine (TBP) for adjusting the conductivity.[21] As an important class of organic HTMs, carbazole-based compounds have been widely investigated in optoelectronic applications owing to their excellent charge-transporting properties apart from interesting photoconductive, photo-refractive, and light-emitting behaviour.[14] Small molecule carbazoles possess many advantages as optoelectronic materials mainly due to their predictable HOMO-LUMO energy levels, which can be easily tuned through chemical substitution, and high thermal stability, rendering them suitable candidates for thermal evaporation.[22] In addition, carbazole, being a cheap raw material, can easily be substituted through simple routes to yield derivatives of high photochemical stability and also it has the ability to quickly form relatively stable radical cations.[23] Furthermore, the insertion of bulkier branched alkyl chain at *N*-heteroatom of the ring promotes significant tilting and packing distortion and tends to reduce the aggregation as well as solubility problems causing improved open-circuit voltage (V_{OC}) in the fabricated device. Also, it was reported that the length of alkyl chains with significant branching influences the HTM solubility in common organic solvents, and thereby influences the film quality.[24] Additionally, the length of alkyl chains significantly affects charge delocalization property, structural planarity, and the hole transport properties of HTM.[25]

Encouraged by this, in the present study, we report the molecular design, synthesis, and characterization of two novel carbazole-based small molecules, **$CZ_{1\text{-}2}$** comprising mono/dimethoxyphenyl and carbazole units as the electron-donating moieties, cyanovinylene groups as the electron-accepting systems with extended π-conjugation. Figure 1 portrays the chemical structures of **$CZ_{1\text{-}2}$**. These molecules were designed with the possible application in PSCs as HTMs. By adopting the simple synthetic strategy, these carbazole derivatives containing methoxy end-capping groups were synthesized from inexpensive starting materials. Because of their easy three-step synthesis as well as facile availability of starting materials, these newly synthesized molecules are expected to be cost-effective HTMs and hence, they are attractive for commercial prospects of PSCs. We used the well-known Knoevenagel condensation method which offers an extremely simple route for their synthesis. Also, the product separated as a precipitate in the reaction mixture can easily be purified using a simple recrystallization technique. Scheme 1 displays the synthetic schemes adopted for the lab-preparation of the target molecules. Structures of all the new intermediates as well as final compounds were determined by

spectroscopy tools and elemental analysis. Their optical properties and FMO levels were evaluated by UV-Visible spectroscopy and photoluminescence (PL) studies. Further, cyclic voltammetric (CV) studies were performed to assess their electrochemical data along with parameters related to thermodynamic driving factors of the processes involved during energy conversion. Furthermore, the molecular geometry, electron distributions, energetic properties and absorption spectra of $\mathbf{CZ_{1-2}}$ were theoretically studied by means of Density Functional Theory (DFT), and Time-Dependent Density Functional Theory (TD-DFT) using Turbomole 7.2V software. Also, their structure-property relationships were discussed.

<Figure 1>

MATERIALS AND METHODS

The commercially available starting materials such as carbazole, sodium hydride, 2-ethylhexyl bromide, phosphorus oxychloride, (3,5-dimethoxyphenyl)acetonitrile, and 4-methoxyphenylacetonitrile were procured from Sigma-Aldrich, Alfa aesar and Spectrochem companies. All the solvents used in the reactions were of synthetic grade (Merck, Loba Chemie and Spectrochem companies) and they were purified by further drying and distillation process. All the reactions were performed under an inert atmosphere and their completion was monitored by the thin-layer chromatography (TLC) technique. The impure products were separated using column chromatography technique by using silica gel (100-200 and 230-400 mesh). The melting points of synthesized molecules were recorded using Stuart SMP10 digital melting point apparatus. The structural elucidation of all the intermediates and final molecules were done by using spectral techniques such as FTIR, ^{1}H NMR, ^{13}C NMR, Mass (ESI) spectroscopy, and elemental analysis. ^{1}H NMR and ^{13}C NMR spectra were recorded on a Bruker AM 400 MHz spectrometer, in $CDCl_3$ and DMSO-d_6 solvents with tetramethylsilane (TMS) as an internal standard. The LCMS and elemental analysis of the synthesized molecules $\mathbf{CZ_{1-2}}$ were obtained from LC-MS6410Q (Agilent Technologies) and Flash EA1112 CHNS elemental analyser (Thermo Scientific), respectively. FT-IR spectra were obtained using Bruker FTIR Alpha spectrometer. The UV-Vis absorption spectra and photoluminescence spectra of $\mathbf{CZ_{1-2}}$ in chloroform solvent were recorded at room temperature by using Analytik Jena SPECORD S 600 and Jasco FP 6200 spectrophotometers, *respectively*. Furthermore, in order to assess their experimental GSOP and

ESOP values, the CV (cyclic voltammetry) measurements were performed in anhydrous acetonitrile solution with 0.1M tetrabutylammonium hexafluorophosphate [TBA] [PF_6] as a supporting electrolyte at a scan rate of 100 mVs^{-1}. The theoretical simulations, *viz.* density functional theory (DFT) and time-dependent density functional theory (TD-DFT), were performed for all the final molecules using the Turbomole V7.2 software package.[61-64]

Synthetic methods

The required intermediates and final target molecules were synthesized using standard synthetic methods and their detailed procedures along with structural characterization data are given below.

*Synthesis of 9-(2-ethylhexyl)-9H-carbazole (**1**).* A mixture of carbazole (0.1 g, 0.598 mmol), NaH (0.07 g, 2.99 mmol) was dissolved in a minimum amount of DMF (5 mL) and stirred at room temperature for half an hour under an inert atmosphere. Later, 2-ethylhexyl bromide (0.34 g, 1.79 mmol) was added into the reaction mixture and continued stirring at room temperature for 12 h. The reaction progress was monitored using thin-layer chromatography (TLC). After completion of the reaction, the reaction mixture was cooled and poured into crushed ice (100 mL) and neutralization was done using a saturated solution of ammonium chloride. The precipitate formed was filtered, washed with ice-cold water and finally, it was recrystallized using ethanol to get colourless liquid as a product. Yield: 92%.

^{1}H NMR (400 MHz, DMSO-d6, δ ppm): 8.47 (s, 1H), 8.00-7.98 (t, 3H), 7.61 (s, 1H), 7.13-7.11 (d, 3H), 4.07-4.05 (d, 2H), 1.73 (s, 1H), 1.24-1.11 (m, 8H), 0.86-0.84 (t, 6H). Anal. Calcd. for $C_{20}H_{25}N$: C, 85.97; H, 9.02; N, 5.01; and found C, 85.89; H, 8.99; N, 5.06. **FT-IR (ATR), υ** cm^{-1}: 3063, 2956 (C-H), 1589, 1533, 1482 (C=C), 1191 (C-N).

*Synthesis of 9-(2-ethylhexyl)-9H-carbazole-3,6-dicarbaldehyde (**2**).* In a cleaned two neck round bottom flask, freshly distilled DMF (1.22 mL, 15.75 mmol) was taken and cooled it at –3 to 4 ºC. Then, phosphorous oxychloride, $POCl_3$ (1.67 mL, 17.90 mmol) was added drop-wise with constant stirring at the same temperature under argon atmosphere to obtain a glassy white salt. To this mixture, 9-(2-ethylhexyl)-9*H*-carbazole (**1,** 0.2 g, 0.71 mmol) dissolved in dichloroethane (2 mL) was added. The reaction mixture was refluxed at 95 ºC for 12 h. After completion of the reaction, the reaction mass was cooled to room temperature and poured into 100 mL crushed ice

and subsequently basified by using 5 M NaOH solution. The product formed was extracted with ethyl acetate (50 mL x 3) and the organic layer was dried over sodium sulphate and evaporated under reduced pressure. The impure residue was later purified by column chromatography on silica gel (100-200 mesh) to yield a light brown solid (**2**). Yield: 69%. Melting point: 104-106 °C.

^{1}H NMR (400 MHz, DMSO-d6, δ ppm): 10.09 (s, 2H), 8.89-8.88 (d, 2H), 8.06-8.04 (q, 2H), 7.82-7.81 (d, 2H), 4.39-4.37 (d, 2H), 1.32-1.29 (d, 1H), 1.14-1.11 (m, 8H), 0.85-0.82 (t, 3H), 0.75-0.72 (t, 3H). Anal. Calcd. for $C_{22}H_{25}NO_2$: C, 78.77; H, 7.51; N, 4.18; and found C, 78.02; H, 7.49; N, 4.13. **FT-IR (ATR), υ** cm^{-1}: 3051, 2956 (C-H), 1681 (C=O), 1587, 1482 (C=C), 1193 (C-N).

*Synthesis of (2Z, 2′Z)-3, 3′-(9-(2-ethylhexyl)-9H-carbazole-3,6-diyl)bis(2-(3,5-dimethoxy phenyl)acrylonitrile) (**CZ$_1$**).* A mixture of 9-(2-ethylhexyl)-9*H*-carbazole-3,6-dicarbaldehyde (**2,** 0.05 g, 0.14 mmol) and potassium *tert*-butoxide (0.27 g, 2.47 mmol) was dissolved in dry methanol (10 mL) and stirred at room temperature under an argon atmosphere for 15 min. Later, (3,5-dimethoxy phenyl) acetonitrile (0.1 g, 0.62 mmol) was added while stirring and the reaction mixture was refluxed for 6 h. The precipitate formed was filtered, washed with absolute methanol and finally, it was recrystallized from chloroform to obtain bright yellow color solid. Yield: 84%. Melting point: 192-194 °C.

^{1}H NMR (400 MHz, DMSO-d6, δ ppm): 8.72 (s, 2H), 8.18-8.15 (t, 4H), 7.80-7.78 (d, 2H), 7.39 (s, 2H), 7.31-7.28 (d, 2H), 7.10-7.08 (d, 2H), 4.37-4.36 (d, 2H), 3.89 (s, 12H), 1.40-1.31 (m, 9H), 1.30-1.26 (t, 6H). **^{13}C NMR** (400 MHz, DMSO-d6, δ ppm): 148.66, 148.29, 141.32, 140.28, 126.92, 126.27, 124.80, 122.06, 121.49, 118.11, 117.76, 110.31, 108.83, 107.55, 107.01, 76.32, 76.20, 76.00, 75.68, 55.08, 55.03, 46.79, 38.49, 29.98, 28.68, 27.78, 23.39, 21.99, 12.99, 9.87. Anal. Calcd. for $C_{42}H_{43}N_3O_4$: C, 77.16; H, 6.63; N, 6.43; and found C, 77.54; H, 6.89; N, 6.41. **FT-IR (ATR), υ** cm^{-1}: 2921 (C-H), 2207 (C≡N), 1592, 1513, 1472 (C=C), 1212 (C-N). **Mass (m/z):** 653.81; Obtained (M+Na)$^+$: 676.31.

*Synthesis of (2Z, 2′Z)-3, 3′-(9-(2-ethylhexyl)-9H-carbazole-3,6-diyl)bis(2-(4-methoxy phenyl) acrylonitrile) (**CZ$_2$**).* A mixture of 9-(2-ethylhexyl)-9*H*-carbazole-3,6-dicarbaldehyde (**2,** 0.05 g, 0.14 mmol) and potassium *tert*-butoxide (0.27 g, 2.47 mmol) was dissolved in dry methanol (10 mL) and stirred at room temperature under an argon atmosphere for 15 min. Later, (4-methoxyphenyl) acetonitrile (0.09 g, 0.62 mmol) was added while stirring and the reaction mixture was refluxed for 6 h. The precipitate formed was filtered, washed with absolute methanol and

finally, it was recrystallized using chloroform to obtain pale orange-yellow color solid. Yield: 79%. Melting point: 178-180 °C.

^{1}H NMR (400 MHz, DMSO-d6, δ ppm): 8.72 (s, 2H), 8.19-8.15 (m, 5H), 7.81-7.79 (d, 3H), 7.39 (s, 2H), 7.31-7.28 (d, 2H), 7.11-7.09 (d, 2H), 4.38-4.36 (d, 2H), 3.89 (s, 3H), 3.82 (s, 3H), 2.04-2.03 (d, 1H), 1.18-1.31 (m, 8H), 0.90-0.86 (t, 3H), 0.80-0.77 (t, 3H). **^{13}C NMR** (400 MHz, DMSO-d6, δ ppm): 160.06, 142.27, 141.08, 127.61, 127.13, 127.08, 125.89, 123.06, 122.55, 119.14, 114.43, 109.81, 107.84, 77.35, 77.24, 77.04, 76.72, 55.46, 47.80, 39.51, 31.01, 28.82, 24.42, 23.02, 14.03, 10.90. Anal. Calcd. for $C_{40}H_{39}N_3O_2$: C, 80.91; H, 6.62; N, 7.08; and found C, 80.76; H, 6.70; N, 7.10. **FT-IR (ATR), υ** cm^{-1}: 3018 (C-H), 2209 (C≡N), 1605, 1510, 1488 (C=C), 1214 (C-N). **Mass (m/z):** 593.30; Obtained: 593

RESULTS AND DISCUSSION

Synthesis and characterization

The synthetic methods of two new products, *viz.* 3,3′-(9-(2-ethylhexyl)-9*H*-carbazole-3,6-diyl)bis(2-(mono/di-methoxy substituted phenyl) acrylonitrile) (**CZ_{1-2}**) are portrayed in Scheme 1**.** The requisite intermediate 9-(2-ethylhexyl)-9*H*-carbazole (**1**) was obtained from *9H*-carbazole by treating it with 2-ethylhexyl bromide in presence of a strong base, *i.e.* sodium hydride. This was converted to the key precursor 9-(2-ethylhexyl)-9*H*-carbazole-3,6-dicarbaldehyde (**2**) through Vilsmeier-Hack reaction in good yield. Finally, compound **2** on reaction with (3,5-dimethoxyphenyl)acetonitrile and (4-methoxyphenyl) acetonitrile by following the Knoevenagel condensation protocol, yielded **CZ_1** and **CZ_2** respectively. All the synthesized compounds were purified further by using a simple recrystallization technique from chloroform solvent. The molecular structures of these target compounds and their intermediates were established by using different spectroscopy tools. Their spectra are displayed in **S1-S11** of ESI.

<Scheme 1>

Theoretical studies

To optimize the ground state geometry of molecules and to obtain an insight into the electronic distribution behavior of compounds **CZ_{1-2}** quantum chemical calculations / Density Functional Theory (DFT) simulations were carried out by employing the Turbomole 7.2v software package. In fact, these computational studies play a key role in designing novel semiconducting materials with proper energy levels as well as good charge mobility. In the present study, we have optimized the ground-state geometries of the newly synthesized **CZ_{1-2}** in a gas phase using a semi-empirical AM1 basis with MOPAC in Tmolex.[26] The further optimization of aforesaid geometries was done with the help of software-generated C_1 point group symmetry *via* B3LYP program and here, the basic set def-TZVPP was used for all the calculations.[27] The obtained electronic cloud distributions in the frontier molecular orbitals (FMOs) levels of **CZ_{1-2}** are shown in Figures 2 and **S12** and the related data are displayed in Table 1. Here, the LUMO+1, and HOMO-1 levels correspond to second-lowest unoccupied molecular orbitals and second-highest occupied molecular orbitals, *respectively*. The effective charge separation between the ground state and excited state of the molecule can be clearly observed in 3-D visions of the molecules.

It has been well-documented that the electron-donating ability of carbazole donor has a greater impact on energy levels and spatial charge distribution of the HOMOs, which further influences the interfacial charge transport. In addition, FMOs are the most widely used to demonstrate the charge transport behaviour of the molecules, as more delocalized FMOs can undergo quicker charge transport by increasing the electron coupling between adjoining molecules and reducing nuclear reorganization energy. As seen in Fig. 2, in case of HOMO levels, the total electron densities of **CZ_{1-2}** are primarily distributed with the donor skeleton, which clearly indicates the electron-donating ability of 9-(2-ethylhexyl)-9*H*-carbazole. In addition to this, electron density also slightly distributed over pendant groups, *i.e.* methoxy phenyl groups. Nevertheless, the electron density distribution in LUMO is mainly localized over electron-withdrawing cyanovinylene moiety. Further, it can be observed that as we move from HOMO to HOMO-1, the electron density is slightly away from donor carbazole to methoxyphenyl groups. Interestingly, the complete shift of electron density towards electron-withdrawing cyanovinylene group has been observed in the LUMO level. The major difference between **CZ_1** and **CZ_2**, lies in their substituent groups, as **CZ_1** has an additional methoxy group suggesting stronger electron-donating capability. The analysis of FMO shows that the excitation of an electron from lower

HOMO to LUMO level results in electron density to surge from electron-donating carbazole and methoxyphenyl units to electron-withdrawing cyanovinylene group, which ultimately influence the charge carrier transport inside the molecule and can create effective charge separation at the donor-acceptor interface. Besides, **CZ_1** has higher HOMO energy as compare to **CZ_2** due to the existence of additional electron-pushing methoxy functionality. Structurally, the location and number of methoxy groups significantly affect the electron-donating ability, thereby increasing the donor strength in **CZ_1**; here, the presence of two electron-releasing methoxy groups at the *meta*-positions with respect to the core (9-(2-ethylhexyl) carbazole-3,6-diyl)diacrylonitrile moiety could facilitate the molecule to achieve higher donor-acceptor interactions than **CZ_2**. Hence, **CZ_1** can be considered as better HTM than **CZ_2** due to the enhanced electron-releasing effect of methoxy groups.

In PSCs, the occurrence of appropriate energy levels between the perovskite and the HTM is absolutely necessary for facilitating effective interfacial charge separation and thereby maximizing the open-circuit voltage (V_{OC}) of the devices. A deeper HOMO level of the molecules usually indicates the larger V_{OC}, since the voltage value is dependent on the difference between HOMO levels of the HTM and quasi-Fermi level of the TiO_2 semiconductor. The theoretical HOMO energy levels obtained for **CZ_1** and **CZ_2** are –5.48, and –5.33 eV, *respectively* confirming these compounds can undergo a quick ground state regeneration process. Generally, for promising HTMs, the value of the LUMO levels must be greater than the conduction band of the perovskite (–3.93 eV for $CH_3NH_3PbI_3$) in order to block the recombination of electrons and holes between perovskite absorber and the metal electrode.[28] The theoretical LUMO energy levels obtained for **CZ_1** and **CZ_2** are –2.01 and –1.92 eV, *respectively*, demonstrating their fast electron injection ability. When compared to the conduction edge of most commonly used perovskite $CH_3NH_3PbI_3$, the LUMOs of **CZ_1** and **CZ_2** give rise to a large energy barrier of 1.92-2.01 eV, indicating that the unwanted electron-hole recombination process could be effectively prohibited. From the results, it is clear that both the molecules possess a capability of photo-induced electron transfer from the HOMO-LUMO excitations. The theoretical bandgaps obtained for **CZ_1** and **CZ_2** are 3.464 and 3.408 eV *respectively*, which may be accredited to the different donating ability in the molecules. Although it is difficult to obtain accurate FMO energies by DFT studies, the changing tendencies between theoretical and experimentally obtained energy values are consistent.

From the energy level alignments and frontier orbital distribution we emphasize that the carbazole donor with branched alkyl chain has been thoughtfully tailored as the side arms of the molecules. On comparing the HOMO levels of the **CZ_{1-2}** with the reported HOMO energy level of *spiro*-OMeTAD (–5.08 eV), our new molecules show comparatively stabilized HOMOs, and hence better hole injection and enhanced V_{OC} values can be expected.[3] Conclusively, the FMO levels of the **CZ_{1-2}** can promise a faster charge-transport between the electron-donor and acceptor units and the well-organized interfacial injection of electrons from the excited level of the HTM into the conduction band (CB) of the semiconductor. Further, the electron distribution pattern in the FMO levels clearly indicates that the molecules **CZ_{1-2}** possess good hole-transporting properties, and hence they may turn out to be promising candidates of HTMs.

<Figure 2>

<Table 1>

In order to gain insights into the excitation properties as well as electronic transition, the light absorption properties were explored using Time-Dependent Density Functional Theory (TD-DFT) in the presence of time-dependent perturbations. According to adiabatic approximation, TD-DFT temporal nonlocality is neglected, which postulates at any point of time, the exchange-correlation (xc) factor depends exclusively on instantaneous density.[29,30] Consequently, it can be utilized to the xc functional derived for ground-state DFT, *i.e.* BP (Beck-Perdew) and hybrid functional (B3LYP). In TD-DFT calculations, the basis set used for the calculations generally decides the accuracy of assimilated results.[31] Figure S13 (see Supporting Information) shows the simulated absorption spectra of **CZ_{1-2}**, obtained by employing B3LYP functional and def-TZVP basis set.[32] The theoretically calculated absorption maxima (λ_{max}) of the investigated molecules **CZ_{1-2}** are summarized in Table 1. The energy values related to long-range charge-transfer states can be predicted precisely using TD-DFT calculations. Further, as shown in Figure S13 the investigated molecules **CZ_{1-2}** show two distinct peaks, corresponding to mixed π-π^* transition and charge-transfer process within the molecules in the visible light region. In all the molecules, there occurs a strong intra-molecule electronic excitation, owing to the HOMO→LUMO and HOMO→LUMO+1 transition. Here, the excitations at the longer wavelengths are due to the electronic transition from the HOMO to LUMO+1 level. Accordingly, the lower-energy

excitations are ascribed to intramolecular charge-transfer (ICT) transitions from **CZ_1** and **CZ_2** to TiO_2. Furthermore, λ_{max} of **CZ_1** (420 nm) shows a noticeable redshift when compared to that of **CZ_2** (400 nm). This may be ascribed to the higher electron-donating strength, as it contains two pendent methoxy groups attached to carbazole *via* cyanovinylene unit. In addition, the oscillator strength (*f*) of **CZ_1** was found to be larger than that of **CZ_2**, which corresponds to the appearance of a larger experimental absorption coefficient or stronger fluorescence intensity. Accordingly, **CZ_1** has a higher absorption intensity than the molecule **CZ_2**. These exactitudes of TD-DFT results demonstrate that the functional and basis set selected for the studies are well in agreement with experimentally obtained results. Theoretically simulated IR-absorption spectra of **$CZ_{1\text{-}2}$** are displayed in Figure S14. As expected, both the simulated and experimentally obtained results are well in accordance with each other.

The distribution of total charge density of an organic molecule at any point in space around the molecule produces a net electrostatic effect. This phenomenon is known as molecular electrostatic potential (ESP). Computationally, molecular ESP simulations were carried out in order to investigate the charge populations of **$CZ_{1\text{-}2}$** and the corresponding plotted ESP maps are shown in Fig.3**.** The cavity boundaries in the molecules resemble the density isosurface in the ESP plot, which is coupled with total charge distribution including electro-negativity, dipole moment as well as site of chemical reactivity of the molecule.[33–35] The electrostatic potential values are denoted by different colors and they increase in the order, blue > green > yellow > orange > red. The electron-rich and electron-deficient regions are represented by red and blue colors on the plot, which induces positive and negative charges on the cavity surface, further giving rise to local electric fields inside the cavity. From Fig.3, it is evident that in molecules **$CZ_{1\text{-}2}$**, the total electron density is mainly concentrated on cyanovinylene, and pendent methoxy groups. Thus, the ESP plots clearly demonstrate the movement of electron density from the donor moiety to the acceptor units, thereby favoring the useful electron transfer in both **$CZ_{1\text{-}2}$**. These results also reveal that introduction of different end-capping methoxy groups lightly affects the stability of the molecules. Further, Laplacian of electron density and ground-state total density of the molecules **$CZ_{1\text{-}2}$** are shown in Figures S15-S16. The structure of the molecule is a mono/dimethoxy phenyl substituted cyanovinylene side arms symmetrically placed at 3rd and 6th positions of a 9-(2-ethylhexyl)-9*H*-carbazole, located at the centre. Studies were made to analyse the charge density and Laplacian of charge density of the molecule, with a little much importance given to the central ring. From these studies, we can figure out the position of bond critical point (BCP), which provides the knowledge

of electronegative nature of atoms and its electron density distribution based on bonding nature.[36] Laplacian of total density is considered as a useful tool for characterizing bonding interactions inside the molecules. In-depth studies of these plots also provide a greater understanding of the electronic properties bounded inside atoms and molecules, delocalization nature, and allow for useful predictions of chemical reactivity.[25]

<Figure 3>

According to quantum mechanics, in a system, the energy levels per unit energy increment correspond to the density of states (DOS). It determines the number of states per specific interval of energy at each energy level, and are free to be occupied.[37-38] In a simpler way, the higher the DOS corresponds to the availability of many states for occupation at a particular energy level, whereas zero DOS indicates the availability of no free states. In general, the DOS is an average over the time and space domains occupied by the system, and it describes the contribution of different orbitals over a different range of energy. The DOS also describes the favorable charge-transfer from a molecule to the TiO_2 semiconductor, which further builds the dipolar fields at the interface of TiO_2/Material to tune the band energy levels.[39] The smaller the bandgap of the material facilitates the faster electron transport from it and thus, increasing the driving force for rapid charge injection at the interface. The DOS plots of **CZ_{1-2}** are depicted in Figures S17-S18. Here, the figures indicate the contribution of different orbitals as energy increases. It is observed from the figure that as the energy increases, the contribution of *p*-orbitals predominates over the *s*-orbitals. It can also be seen that the *p*-orbital contribution of *O* and *N* atoms facilitates the binding of dye with TiO_2. Both the new molecules show a similar pattern of DOS maps indicating that they meet the prerequisites of a good HTM. Further, DOS spectra of dyes did not show a prominent energy gap but the obtained results are well in accordance with literature reports.[40] Both the molecules exhibit significant charge-transfer from donor to acceptor unit confirming that they meet the basic requirements of an ideal HTM.

Photophysical properties

The UV-vis absorption spectra of newly synthesized **CZ_{1-2}** were obtained in chloroform ($CHCl_3$) solution with a concentration of 10^{-5} M at room temperature. Their generated spectra are

displayed in Fig.4a and the corresponding data are tabulated in Table 2. These spectra exhibit two distinct absorption peaks, of which the lower maximum represents π-π* electronic excitation occurring in the range of 300-350 nm, whereas the higher maximum, appearing at 400-430 nm corresponds to the electronic transition from HOMO to LUMO and HOMO-1 to LUMO. Both the molecules show absorption bands comparable to that of spiro-OMeTAD (388-390 nm),[41-43] and hence it can be inferred that their optical properties are matching with that of commercially available HTM.[44,45] As shown in Fig.4a, both **CZ_{1-2}** exhibit similar type of absorption profiles and the observed major λ_{max} of **CZ_1** is 428 nm, and that of **CZ_2** is 417 nm. Here, the peaks are due to mixed intra-molecular charge transfer (ICT) / π-π*transition of the compounds, which was further confirmed by TD-DFT calculations.[46] From the results, we infer that **CZ_1** shows a bathochromic shift when compared to the spectral data of **CZ_2**, which may be due to the presence of an additional electron-donating pendent group that further extends the conjugation of **CZ_1**. It is also well-known that the number and position of the methoxy groups make a significant influence on the geometrical structure and subsequently on the electronic properties of the molecules, which means that the presence of more pendant methoxy groups augments the electron-donating ability of the molecule, and thus providing superior performance.[47] Also, its position significantly affects the planarity and hence, geometries of such molecules. In our molecules, positioning of the two methoxy groups at the *meta*-positions will cause a lower steric hindrance than positioning them at the *ortho-ortho*/*ortho-para*/*ortho-meta* positions.[48,49] For instance, in **CZ_1**, the two methoxy groups are placed at the meta-positions showing smaller conformational changes in the excited state. Hence, we have chosen (3,5-dimethoxyphenyl) acetonitrile as dual pendant group for **CZ_1** rather than (3,4-dimethoxyphenyl)acetonitrile or (2,4-dimethoxyphenyl)acetonitrile moieties. Further, from the literature, it is evident that the position of methoxy groups can control the oxidation potential of the materials, and hence their electronic properties are affected by the position of methoxy substituents.[50] The change in the substitution from *para* to *meta* results in increased oxidation potential of the material due to the less electron-donating nature of *m*-OMe groups when compared to that of *p*-OMe group. Also, the *meta*-substituted derivatives could decrease the HOMO energy level of the HTM, and thus may contribute to an increase in open-circuit voltage and fill factor of the resulting PSCs.[51]

Further, the molar extinction coefficients of molecules **CZ_{1-2}** were determined according to Lambert-Beer law (the detailed procedure is given in the ESI). The molar extinction coefficients

of **CZ_{1-2}** were found to be 21,300 $M^{-1}cm^{-1}$ (**CZ_1**) and 20,400 $M^{-1}cm^{-1}$ (**CZ_2**) indicating their good light-harvesting capability. Among both, **CZ_1** shows a higher molar extinction coefficient than **CZ_2** which may be owing to the stronger electron-donating ability of dual methoxy pendent units towards carbazole scaffold. So, from the results, we can conclude that **CZ_1** shows an improved light-harvesting ability and hence it can be considered as a better HTM.

The fluorescence emission spectra of molecules were measured in 10^{-5} M $CHCl_3$ solution by exciting at their respective absorption maxima. Figure 4b portrays the normalized emission spectra of **CZ_{1-2}** and their resulting spectral parameters are tabulated in Table 2. Both the molecules exhibit a characteristic single emission band in the region of 530-560 nm. The molecule **CZ_1** displays λ_{emi} of 557 nm, which is slightly more red-shifted than that of **CZ_2** (536 nm), which may be due to the strong electron-donating ability of dimethoxyphenyl group. Further, we calculated Stokes shift values as well as the optical bandgap from the experimentally obtained UV-PL spectral data. Indeed, the Stokes shift plays a key role in deciding whether the synthesized HTMs would undergo any geometrical change on excitation. The intersection of absorption and emission spectra of **CZ_{1-2}** is shown in Figure S19. The calculated bandgaps are 2.52 eV (**CZ_1**), and 2.58 eV (**CZ_2**), whereas Stoke shifts are in the order **CZ_2** (5323cm^{-1}) < **CZ_1** (5410cm^{-1}). Here, **CZ_1** shows a higher Stokes shift value with appropriate bandgap and thus, it plays a pivotal role in the light-harvesting phenomenon and it is considered to be better hole-transporting material.

<Figure 4>

<Table 2>

Further, the solvatochromic behavior of **CZ_{1-2}** in solvents of different polarities was investigated in order to understand the deeper insight of intramolecular charge transfer (ICT) phenomenon inside the molecules.[52] The UV-vis absorption and fluorescence emission spectra of synthesized compounds were measured in five different solvents with varying solvent polarities such as toluene, THF, DCM, DMF, and acetonitrile medium at a concentration of 10^{-5} M at room temperature. The solvatochromic absorption spectra of **CZ_1** and **CZ_2** in five solvents having

different polarity ratio starting from highly non-polar toluene to extremely polar DMF and acetonitrile at micro-molar concentration are manifested in Figures 5a-b. It has been noticed that there is noticeable variation in the absorption spectra of the molecules with increasing polarity, indicating an effective dipole moment and non-polar ground state associated with it. Yet, all the molecules exhibit a monotonic bathochromic shift with the increasing polarity of solvents. As seen in the spectra, the molecule **CZ_1** (429 nm) shows an enhanced positive solvatochromic absorption in all the solvents, particularly in the highest polar acetonitrile, when compared to **CZ_2** (420 nm). In addition, from Fig.5, it is clear that both **$CZ_{1\text{-}2}$** display minor hypsochromic shift in less polar and higher vibrational-resolution solvents such as toluene, THF, DCM when compared to $CHCl_3$. The largest blue-shift is observed for THF and toluene (4 and 3 nm *respectively* for **CZ_1**, and 7 and 4 nm *respectively* for **CZ_2**). Such behavior is characteristic of the donor-acceptor conjugated systems.[53] Further, they display a slight bathochromic shift in polar solvents such as DMF and acetonitrile when compared to $CHCl_3$. This unusual redshift in polar solvents arises from the effective solvation of the molecules, induced by the instant stabilization of polarizable electrons during the electronic excitation.[54] This observation clearly indicates that with increasing the solvent polarity, the energy of the ground state is lowered less than that of the excited state.[55] From the results, it is worth noting that there exists a prominent intramolecular charge transfer from the donor moiety towards the electron acceptor unit in the excited state of the molecule, demonstrating **$CZ_{1\text{-}2}$** exhibit a polar excited state with a largely associated dipole moment.

<Figure 5>

Figure 6a-b displays the fluorescence emission spectra of **$CZ_{1\text{-}2}$** in five solvents owing to different polarity ratio. With increasing solvent polarity, there is a considerable change in the emission spectra of all the molecules at the same conditions. Interestingly, the molecule **CZ_1** (565 nm) shows a higher emission intensity than that of **CZ_2** (542 nm), which can be pragmatic through the naked eyes with the colours changing from dark yellow (**CZ_1**) to pale yellow (**CZ_2**) as shown in Fig.6c. The increased emission in **CZ_1** is likely due to the presence of an additional methoxy group which provides an additional donating effect towards carbazole donor that further boosts the conjugation to a greater extent. The Stokes shift values of **$CZ_{1\text{-}2}$** in all the five solvents were calculated and the corresponding results are tabulated in Table 3. Hence, the results demonstrate

that both the compounds display satisfactory positive solvatochromism and can be used as an efficient light-harvesting source in perovskite solar cells. Figure 6d shows the emission behavior of **CZ_{1-2}** solutions under 360 nm UV light.

<Figure 6>

<Table 3>

The solvatochromism can be well-explained by establishing the correlation between the emission nature of **CZ_{1-2}** with solvent variables by using Lippert-Mataga plots (Fig.7) and graphs of E_T (30) index of solvent *vs*. Stokes shift values (Figure S20). Evidently, these two graphs explain progressive linear relationships, which demonstrate the presence of a single excited state with a little deviation in Stokes shift values of these HTMs. Moreover, the observed large Stokes shift values, high positive slope, and linear correlation coefficient (R) of **CZ_1** clearly indicate the comparably higher dipole moment of the excited state than that of the ground state. Hence, these results confirm that the **CZ_1** exhibits stronger intramolecular charge transfer from donor to acceptor moieties than **CZ_2**.

<Figure 7>

Thermal properties

The thermal properties of the compounds **CZ_{1-2}** were investigated by thermogravimetric analysis (TGA). The samples were heated at the uniform heating rate of 10 °C min^{-1} under an inert (N_2) atmosphere. The TGA plots of **CZ_{1-2}** are manifested in Fig.8. Both the synthesized molecules exhibit satisfactory thermal stability with high reasonably thermal decomposition (T_d) temperatures at 245 °C (**CZ_1**), and 236 °C (**CZ_2**). The quantity of carbonized residue was found to be less than 1% at 800 °C in a nitrogen atmosphere, due to their moderate aromatic content (Figure S21). The **CZ_1** shows higher thermal stability than **CZ_2**, making it more relevant material for electronic/photonic applications. Thus, because of their promising thermal property, their application as HTM would impart enhanced stability to the fabricated devices.

<Figure 8>

Electrochemical characterization

The feasibility of thermodynamically allowed transfer of electrons from the excited state of any HTM to the conduction band (CB) of semiconductor and its regeneration by blocking the charge recombination between oxidized materials and photo-injected electrons in CB of TiO_2 can be effectively studied using cyclic voltammetry studies (CV).[56,57] The CV studies are performed for **CZ$_{1\text{-}2}$** using a conventional three-electrode system, in which platinum disc, glassy carbon, and Ag/AgCl serve as passive, working, and reference electrodes, *respectively*.[58] The potentials are measured at a scan rate of 100 mVs^{-1} using supporting electrolyte, tetra *n*-butylammonium hexafluorophosphate in acetonitrile solution in an ambient atmosphere. The generated voltammograms of **CZ$_{1\text{-}2}$** are depicted in Figure S22. From the experimental CV data, we have calculated ground state oxidation potential (GSOP)/HOMO energy levels from the onset oxidation potential of the oxidation peak using equation (1) and the values obtained for both the molecules are summarized in Table 4. Accordingly, they were found to be –5.37eV (**CZ$_1$**), and –5.39eV (**CZ$_2$**), *respectively*.

$$HOMO = -[E_{onset}^{oxd} + 4.7\ eV] \quad (1)$$

$$LUMO = E_{0-0} + HOMO \quad (2)$$

The experimental GSOP/HOMO values of **CZ$_{1\text{-}2}$** are in between that of $CH_3NH_3PbI_3$ (–5.43 eV) and Au counter electrode (–5.1 eV), suggesting that both the molecules can provide a driving force for their quick ground state regeneration. Further, the exited state oxidation potential (ESOP)/LUMO values were calculated from their GSOP values, and optical band gaps $E_{0\text{-}0}$ and respective values in volts (V) against NHE were converted into electron volt (eV) using the equation (2). Table 4 depicts the estimated ESOP values of **CZ$_{1\text{-}2}$** and Fig.9 shows the pictorial representation of their energy level diagram. As seen from the table, their ESOPs are –2.85eV(**CZ$_1$**), and –2.81eV(**CZ$_2$**), which are greater than the conduction band edge of $CH_3NH_3PbI_3$(–3.93eV), and hence they can block electron transport from perovskite to the Au counter electrode easily.[59,60] Thus, both the molecules satisfy the stringent requirement which is mandatory for the affirmative transition of charges throughout the photo-electronic conversion cycle. The generated radical cation of the carbazole moiety is stabilized due to the di-substitution in the 3,6-positions of the molecule which ultimately leads to the first quasi-reversible system. Based on these results, we can conclude that both **CZ$_{1\text{-}2}$** are potential hole-transporting candidates

in $CH_3NH_3PbI_3$ based solar cells. Here, **CZ_1** has more appropriate energy levels than that of **CZ_2**, which mediates holes from $CH_3NH_3PbI_3$ perovskite to Au counter electrode due to the higher donating capacity of dimethoxy groups on **CZ_1**. Also, the introduction of pendant groups improves the oxidation potential of the compounds due to the inductive effect caused by the terminal methoxy groups. Thus, **$CZ_{1\text{-}2}$** satisfies the basic requirements of potential HTM, which further facilitate the affirmative transition of charges throughout the photo-electronic conversion cycle.

<Figure 9>

<Table 4>

CONCLUSION

In summary, we designed two new push-pull type 9-(2-ethylhexyl)-9*H*-carbazole-based **$CZ_{1\text{-}2}$** bearing mono/dimethoxyphenyl substituted cyanovinylene units in its 3rd and 6th positions symmetrically, as potential HTMs for PSC application. The simplicity of their synthesis from available commercial products and easy purification steps offer a cost-effective and scalable route. Their photophysical, thermal as well as electrochemical properties were probed systematically and the effect of structural modification on their properties has been discussed in-depth. Our results demonstrate that their absorption and emission are in the range of 410-430 nm and 530-560 nm, *respectively* with a bandgap of 2.5-2.6 eV, nearly matching to that of perovskite. Further, they have been comprehensively evaluated using quantum chemistry simulations on the basis of DFT and TD-DFT studies and the results strongly support their high charge transfer efficiency. The results clearly indicate that **$CZ_{1\text{-}2}$** meet the basic prerequisites of an ideal HTM making them highly suitable for PSC application. Thus, our outcomes suggest new design strategies for low-cost and effective hole transport materials, and also provide the guiding principle on the structural design of small organic molecules.

Acknowledgements

The authors are grateful to the Director, NITK, Surathkal, India, for providing necessary laboratory facilities.

Declaration of Competing Interest

The authors declare that they do not have known competing financial interests or personal relationships that could have appeared to affect the work reported in this paper.

SUPPORTING INFORMATION

Additional supporting information may be found online in the Supporting Information section at the end of the article:

Figure S1. FT-IR spectrum of intermediate **2**

Figure S2. FT-IR spectrum of **CZ_1**

Figure S3. FT-IR spectrum of **CZ_2**

Figure S4. ^{1}H-NMR spectrum of intermediate **1** recorded in DMSO-d_6

Figure S5. ^{1}H-NMR spectrum of intermediate **2** recorded in DMSO-d_6

Figure S6. ^{1}H-NMR spectrum of **CZ_1** recorded in DMSO-d_6

Figure S7. ^{1}H-NMR spectrum of **CZ_2** recorded in DMSO-d_6

Figure S8. ^{13}C-NMR spectrum of **CZ_1** recorded in DMSO-d_6

Figure S9. ^{13}C-NMR spectrum of **CZ_2** recorded in DMSO-d_6

Figure S10. LCMS spectrum of **CZ_1**

Figure S11. LCMS spectrum of **CZ_2**

Figure S12. Optimized geometries and frontier molecular orbitals (HOMO and LUMO) of **CZ_{1-2}**

Figure S13. Theoretical and experimental electronic excitation spectra of **CZ_1** and **CZ_2**

Figure S14. Theoretical and experimental FT-IR spectra of **CZ_1** and **CZ_2**

Figure S15. Theoretically obtained ground state total density plots of **CZ_1** and **CZ_2**

Figure S16. Theoretically obtained Laplacian of total density plots for **CZ_1** and **CZ_2**

Figure S17. DOS plot of **CZ_1**

Figure S18. DOS plot of **CZ_2**

Figure S19. Intersection of UV-Vis absorption and fluorescence emission spectra of **CZ_{1-2}** recorded in 10^{-5} M $CHCl_3$ solution under ambient atmosphere

Figure S20. Plots showing E_T (30) index of solvent *vs.* Stokes shift of (**a**) **CZ_1** and (**b**) **CZ_2**

Figure S21. Thermograms of **CZ_{1-2}** obtained under N_2 atmosphere at 10 °C min^{-1} heating rate

Figure S22. CV traces of **CZ_1** and **CZ_2**

References

[1] a) Kojima, A., K. Teshima, Y. Shirai and T. Miyasaka (2009) Organometal Halide Perovskite as Visible-light Sensitizers for Photovoltaic Cells. *J. Am. Chem. Soc.* **131***,* 6050; b) Bakr, Z. H., Q. Wali, A. Fakharuddin, T.M. Brown and R. Jose (2017) Advances in hole transport materials engineering for stable and efficient perovskite solar cells. *Nano energy* **34**, 271-305.

[2] a) Rodr, C., L. Cabau, A. Vidal-ferran and E. Palomares (2018) Advances in the Synthesis of Small Molecules as Hole Transport Materials for Lead Halide Perovskite Solar Cells. *Acc. Chem. Res.* **51**, 869-880.

[3] Reddy, S. S., K. Gunasekar, J. H. Heo, S.H. Im, J. H. Moon and J. Y. Lee (2016) Highly Efficient Organic Hole Transporting Materials for Perovskite and Organic Solar Cells with Long-Term Stability. *Adv. Mater.* **28,** 686-693.

[4] Zhao, X. and M. Wang (2017) Organic hole-transporting materials for efficient perovskite solar cells. *Mater. Today Energy* 1–13.

[5] Zhu, L., Y. Shan, R. Wang, D. Liu and C. Zhong (2017) High Efficiency Perovskite Solar Cells Based on New TPE Compounds as Hole Transport Materials: Role of 2,7- and 3,6-substituted Carbazole Derivatives *Chem. Eur. J* **23.**

[6] Liang, X., K. Wang, R. Zhang, K. Li, X. Lu, K. Guo, H. Wang, Y. Miao, H. Xu and Z. Wang (2017) Hole-transporting materials with high thermal stability and mobility for efficient OLEDs. *Dyes Pigm.* **139**, 764–771.

[7] Keremane, K.S., S. Prathapani, L. Jia, D. Bahulayan, A. V. Adhikari and S. G. Mhaisalkar (2020) Solvent selection for highly reproducible carbon-based mixed-cation hybrid lead halide perovskite solar cells via adduct approach. *Sol. Energy* **199**, 761–771.

[8] Sorkhabi, A. H., P. Salehi-abar, E. Asghari and A. Kazempour (2019) Structural effect on the thermodynamic and electrochemical properties of pyrene-based hole transport materials. *J. Mol. Liq.* **285**, 338–346.

[9] Zheng, X., B. Chen, J. Dai, Y. Fang, Y. Bai, Y. Lin, H. Wei, X.C. Zeng and J. Huang (2017) quaternary ammonium halide anions and cations. *Nature* **17102**, 1–9.

[10] Chi, W., Q. Li and Z. Li (2016) Effect of thiophene chain lengths on the optical and hole transport properties for perovskite solar cells. *Synth. Met.* **211**, 107–114.

[11] Lv, S., Y. Song, J. Xiao, L. Zhu, J. Shi, H. Wei, D. Li, X. Li and Q. Meng (2015) Simple Triphenylamine-Based Hole-Transporting Materials for Perovskite Solar Cells. *Electrochim. Acta* **182**, 733–741.

[12] Michaleviciute, A., M. Degbia, A. Tomkeviciene and B. Schmaltz (2014) Star-shaped carbazole derivative based efficient solid-state dye sensitized solar cell. *J. Power Sources* **253,** 230–238.

[13] Yin, X., L. Guan, J. Yu, D. Zhao, C. Wang, N. Shrestha, Y. Yan and W. Tang (2017) One-step facile synthesis of simple carbazole-cored hole transport material for high performance perovskite solar cells. *Nano energy* **40**, 163-169.

[14] Sathiyan, G., E.K.T. Sivakumar, R. Ganesamoorthy, R. Thangamuthu and P. Sakthivel (2015) Review of Carbazole Based Conjugated Molecules for Highly Efficient Organic Solar Cell Application. *Tetrahedron Lett.* **57**, 243–252.

[15] Wu, F., Y. Shan, X. Li, Q. Song and L. Zhu (2016) Effect of dimethylamino substituent on tetraphenylethylene-based hole transport material in perovskite solar cells. *Org. Electron.* **39**, 323–327.

[16] Wang, Y., Z. Jiang and L. Liao (2016) New advances in small molecule hole-transporting materials for perovskite solar cells. *Chin. Chem. Lett.* **27,** 1293–1303.

[17] Abdellah, I. M., T. H. Chowdhury, J. J. Lee, A. Islam, A. El-Shafei (2020) Novel dopant-free hole-transporting materials for efficient perovskite solar cells. *Sol. Energy* **206,** 279-286.

[18] Liu, X., C. Huang and M. Li (2017) Different p-bridges as hole-transporting materials for efficient perovskite solar cells. *Dyes Pigm.* **139**, 283–291.

[19] Zong, X., W. Qiao, Y. Chen, Z. Sun, M. Liang and S. Xue (2017) A new binaphthol based hole-transporting materials for perovskite solar cells. *Tetrahedron* **73**, 3398–3405.

[20] Daskevicience, M., S. Paek, Z. Wang, K.T. Cho, H. Snaith and M. K. Nazeeruddin (2017) Carbazole-based enamine: low-cost and efficient hole transport material for perovskite solar cells. *Nano energy* **32.**

[21] Mora, J. U., I. G. Benito and N. Martin (2018) Hole transporting materials for perovskite solar cells: a chemical approach. *Chem. Soc. Rev*. **47**, 8541.

[22] Wang, J., Y. Chen, F. Li, X. Zong, J. Guo, Z. Sun and S. Xue (2016) A new carbazole-based hole-transporting material with low dopant content for perovskite solar cells. *Electrochim. Acta* **210***,* 673–680.

[23] Yang, S., W. Fu, Z. Zhang, H. Chen and C. Z. Li (2017) Recent advances in perovskite solar cells: efficiency, stability and lead free perovskite. *J. Mater. Chem.* A **5**, 11462.

[24] Kumari, N., S.R. Patel and J. V. Gohel (2018) Current progress and future prospective of perovskite solar cells: a comprehensive review. *Rev. Adv. Mater. Sci.* **53,** 161-186.

[25] Nh, C. H., P. Huang, Y. Wang, J. Ke and C. Huang (2017) The Effect of Solvents on the Performance. 1–8. https://doi.org/10.3390/en10050599.

[26] Naik, P., K.S. Keremane, M.R. Elmorsy, R. Su and A. El-shafei (2018) Highly efficient carbazole based co-sensitizers carrying electron deficient barbituric acid for NCSU-10 sensitized DSSCs. *Sol. Energy* **169,** 386–391.

[27] Teh, C.H., R. Daik, E.L. Lim, C.C. Yap, N.A. Ludin and M.A.M. Teridi (2016) A review of organic small molecule-based hole-transporting materials for meso-structured organic-inorganic perovskite solar cells. *J. Mater. Chem. A* **4,** 15788.

[28] Babu, D.D., R. Su, A. El-Shafei, A. V. Adhikari (2016) From Molecular Design to Co-sensitization; High performance indole based photosensitizers for dye-sensitized solar cells. *Electrochim. Acta* **198***,* 10-21.

[29] Becke, A. D. (1993) Density-functional thermochemistry. III. The role of exact exchange. *J. Chem. Phys.* **98**, 1372-1377.

[30] Lee, C., W. Yang and R. G. Parr (1998) Development of the Colle-Salvetti correlation-energy formula into a functional of the electron density. *Phys. Rev. B* **37,** 785-789.

[31] Naik, P., R. Su, M. R. Elmorsy, D. D. Babu, A. V. Adhikari (2017) Molecular design and theoretical investigation of new metal-free heteroaromatic dyes with D-π-A architecture as photosensitizers for DSSC application. *J. Photochem. Photobiol. A* **345,** 63-73.

[32] Jin, R., X. Zhang and W. Xiao (2020) Theoretical Studies of Photophysical Properties of D-π-A-π-D-Type Diketopyrrolopyrrole-Based Molecules for Organic Light-Emitting Diodes and Organic Solar Cells. *Molecules* **25,** 667.

[33] Mahmood, A., Y. J. Hu and E. Zhou (2018) Recent progress of porphyrin-based materials for organic solar cells. *J. Mater. Chem. A* **6***,* 16769-16797.

[34] Wojcik, J., P. Kus and R. Wrzalik (2013) Theoretical investigation of porphyrin-based photosensitizers with enhanced NIR absorption. *Phys. Chem. Chem.* **15,** 19651-19658.

[35] Park, J., D. Kim, H.Y. Chung and S.Y. Park (2017) Conjugated polymer for High-performance organic solar cells with small energy loss and high quantum effeciency. *J. Mater. Chem. A* **5,** 16681-16688.

[36] Srinivasan, P. and A. David Stephen (2015) DFT and Bader's AIM analysis of 2, 5-, diphenyl-1, 3, 4-oxadizole molecule: A organic light emitting diode (OLED). *J. Theor. Comput. Chem*. **14(5)***,* 1-13.

[37] Chen, J., Q. Liu, H. Li, Z. Zhao, Z. Lu and Y. Huang (2018) Density Functional Theory Investigations of D-A-D Structural Molecules as Donor Materials in Organic Solar Cell. *Front Chem.* **6**, 1-10.

[38] Zheng, J., Y. Fang, Y. Zuo, S. Diego and Y. Duan (2015) How to Optimize the Interface between Photosensitizers and TiO2 Nanocrystals with Molecular Engineering to Enhance Performances of Dye- Sensitized Solar Cell. *ACS Appl. Mater. Interfaces* **7**, 25341-25351.

[39] Nemudzivhadi, H., N. E. Maluta, R. R. Maphanga and V. Sankaran (2017) DFT calculations of Anatase TiO 2 (1 0 1) Surface Doped with Ruthenium for Application in Dye Sensitised Solar Cell. *J. Phys.: Conf. Ser.* **905**, 012013.

[40] Zheng, J. and M. S. Wong (2015) How to Optimize the Interface between Photo sensitizers and TiO2 Nanocrystals with Molecular Engineering to Enhance Performances of Dye-Sensitized Solar Cells. *ACS applied material. Interfaces* **7***,* 25341–25351.

[41] Hua, Y., P. Liu, Y. Li, L. Sun and L. Kloo (2018) Composite Hole-Transport Materials Based on a Metal-Organic Copper Complex and Spiro-OMeTAD for Efficient Perovskite Solar Cells. *Solar RRL* 1700073.

[42] Liu, J., Y. Wu, X. Yang, K. Zhang and L. Han (2014) A dopant-free hole-transporting material for efficient and stable perovskite solar cells. *Energy Environ. Sci*. **7,** 2963- 2967.

[43] Park, S., J. H. Heo, C. H. Cheon and H. J. Son (2015) A [2,2]paracyclophane triarylamine-based hole-transporting material for high performance perovskite solar cells. *J. Mater. Chem. A* **3,** 24215-24220.

[44] Keremane, K. S., P. Naik and A.V. Adhikari (2020) Simple thiophene based organic dyes as active photosensitizers for DSSC application. *J. nano electron. phys.* **12,** 02039.

[45] Li, H., X. Zheng, Q. Zhang, Z. Li, Y. Hao and G. Fang (2017) Low-cost Carbazole-based Hole Transport Material for Highly Efficient Perovskite Solar Cells. *chemsuschem* **10**. https://doi.org/10.1002/cssc.201700678.

[46] Meier, H., Z. Huang and D. Cao (2017) Metal-free organic dyes for efficient dye-sensitized solar cells. *J. Mater. Chem. C* **5**, 9828–9837.

[47] Chen, Y. C., J. H. Yen, C. L. Chung and C. O. Chen (2019) Methoxy groups on bifluorenylidene-based hole transporting materials result in highly efficient and stable dopant-free inverted perovskite solar cells. *Sol. Energy* **179***,* 371-379.

[48] Wazzan, N. and Z. Safi (2019) Effect of number and position of methoxy substituents on fine-tuning the electronic structures and photophysical properties of designed carbazole-based holetransporting materials for perovskite solar cells: DFT calculations. Arab. *J. Chem.* **12**, 1-20.

[49] Tiazkis, R., T. Malinauskas, M. Saliba and M. K. Nazeeruddin (2017) Methoxydiphenylaminesubstituted fluorene derivatives as hole transporting materials: role of molecular interaction on device photovoltaic performance. *Sci. Rep*. **7**, 150.

[50] Jeon, N. J., H. G. Lee, J. Lee and S. I. Seok (2014) o-Methoxy Substituents in Spiro-OMeTAD for Efficient Inorganic–Organic Hybrid Perovskite Solar Cells. *J. Am. Chem. Soc.* **136(22)***,* 7837-7840.

[51] Wu, F., J. Liu, G. Wang, Q. Song and L. Zhu (2016) *Chem. Eur. J* **22.**

[52] Raju, T. B., S. S. Soni and P.K. Iyer (2019) The solvatochromism and aggregation-induce enhanced emission of triphenylamine substituted styrene derivatives and its application in dye sensitized solar cells. *J. Photochem. Photobiol. A* **376**, 12-21.

[53] Alemán, E. A., J. Joseph and D. A. Modarelli (2015) Solvent Effects on the UV-Vis Absorption Properties and Tautomerism of N-Confused Tetraphenylporphyrin. *J. Org. Chem*. **80 (21)**, 11031-11038.

[54] Frizon, T. E. A., A. A. Vieira, S. Saba, T. Cazati and J. Raflque (2020) Synthesis of 2,1,3-Benzoxadiazole Derivatives as New Fluorophores—Combined Experimental, Optical, Electro, and Theoretical Study. *Front. Chem*. **8**.

[55] Domagalska, B. W. and S. Wysockib (2003) Experimental and theoretical studies on solvent effects of amphiphilic conjugated polyenals. *Phys. Chem. Chem. Phys*. **5**, 696–702.

[56] Babu, D. D., P. Naik and K.S. Keremane (2020) A simple DA-π-A configured carbazole based dye as an active photo-sensitizer: A comparative investigation on different parameters of cell. *J. Mol. Liq*. **310,** 113189.

[57] Abdellah, I. M. and A. El-Shafei (2020) Synthesis and characterization of novel tetra anchoring A2-D-D-D-A2 architecture sensitizers for efficient dye-sensitized solar cells. *Sol. Energy* **198,** 25-35.

[58] Wang, J., Y. Chen, M. Liang, G. Ge, R. Zhou and S. Xue (2016) A new thermal-stable truxene-based hole transporting material for perovskite solar cells. *Dyes Pigm.* **125**, 399-406.

[59] Duan, T., K. Fan, T. Peng, C. Zhong, Y. He and X. Chen (2016) V-shaped organoc dyes with triphenylamine core. *Synth. Met.* **211**, 19-24.

[60] Xu, L., P. Huang, J. Zhang and X. Jia (2017) Methylthiophenylamine-Substituted (2-Ethylhexyl) -9H-Carbazole : A Simple , Dopant-Free Hole- Transporting Material for Planar Perovskite Solar Cells. *J. Phys. Chem. C* **40,** 21821-21826.

[61] Becke, A. D. (1993) Density-functional thermochemistry. III. The role of exact exchange. *J. Chem. Phys*. **98**, 1372-1377.

[62] Lee, C., W. Yang and R. G. Parr (1998) Development of the Colle-Salvetti correlation-energy formula into a functional of the electron density. *Phys. Rev. B* **37,** 785-789.

[63] Naik, P., R. Su, M. R. Elmorsy, D. D. Babu, A. V. Adhikari (2017) Molecular design and theoretical investigation of new metal-free heteroaromatic dyes with D-π-A architecture as photosensitizers for DSSC application. *J. Photochem. Photobiol. A* **345,** 63-73.

[64] Jin, R., X. Zhang and W. Xiao (2020) Theoretical Studies of Photophysical Properties of D-π-A-π-D-Type Diketopyrrolopyrrole-Based Molecules for Organic Light-Emitting Diodes and Organic Solar Cells. *Molecules* **25,** 667.

FIGURE CAPTIONS

Scheme 1. Synthetic routes for the compounds **CZ_1** and **CZ_2**: (i) 2-Ethylhexyl bromide, NaH, DMF, RT, 12 hours (ii) $POCl_3$, DMF, 95 °C, 12 hours (iii) (3,5-Dimethoxyphenyl) acetonitrile, potassium *tert*-butoxide, methanol, 60 °C, 6 hours (iv) (4-Methoxyphenyl) acetonitrile, potassium *tert*-butoxide, methanol, 60 °C, 6 hours

Figure 1. Chemical structures of **CZ_1** and **CZ_2**

Figure 2. The electronic cloud distributions in the FMO levels of **CZ_1** and **CZ_2**

Figure 3. ESP mapping on isodensity surface of molecules **(a) CZ_1, (b) CZ_2**

Figure 4. (a) Normalized UV-Vis absorption and (b) fluorescence emission spectra of **CZ_{1-2}** recorded in 10^{-5} M $CHCl_3$ solution under ambient atmosphere

Figure 5. Normalized UV-vis absorption spectra of **(a) CZ_1**, and **(b) CZ_2** in solvents with varying polarity index

Figure 6. Normalized emission spectra of **(a) CZ_1**, **(b) CZ_2** in solvents with varying polarity index, **(c)** Emission under visible spectrum, and **(d)** Emission under 360 nm UV light

Figure 7. Lippert-Mataga correlation plots of (**a**) **CZ_1** and (**b**) **CZ_2**

Figure 8. Thermograms of **CZ_{1-2}** obtained under N_2 atmosphere at 10 °C min^{-1} heating rate

Figure 9. Molecular energy level diagram showing experimental HOMO, LUMO, and bandgap values of **CZ_1** and **CZ_2**

Table 1. Theoretical electrochemical data of $\mathbf{CZ_1}$ and $\mathbf{CZ_2}$

Molecules	$\mathbf{E_{HOMO}}$ **(eV)**	$\mathbf{E_{HOMO-1}}$ **(eV)**	$\mathbf{E_{LUMO}}$ **(eV)**	$\mathbf{E_{LUMO+1}}$ **(eV)**	$^{a}\mathbf{E_g}$ **(eV)**	$\boldsymbol{\lambda_{max}}$ **(nm)**	**Oscillator strength (f)**
$\mathbf{CZ_1}$	–5.48	–5.85	–2.01	–1.78	3.464	420	0.40
$\mathbf{CZ_2}$	–5.33	–5.68	–1.92	–1.70	3.408	400	0.33

[a]The values obtained in DFT calculations to vacuum

Table 2. Photophysical characterization data of **CZ_1** and **CZ_2**

Molecules	**λ_{abs}[a] (nm)**	**λ_{emi}[b] (nm)**	**Stokes shift (cm^{-1})**	**ε ($M^{-1}cm^{-1}$) at λ_{abs} (nm)**	**$E_{0\text{-}0}$[c], Optical (eV)**
CZ_1	428	557	5410	21,300	2.52
CZ_2	417	536	5323	20,400	2.58

[a] Absorption spectra measured in $CHCl_3$ (at concentration of 10^{-5} M) at room temperature

[b] Emission spectra measured in $CHCl_3$ (at concentration of 10^{-5} M) at room temperature

[c] Optical band gap $E_{0\text{-}0}$ is the voltage of intersection point between absorption and emission spectra

Table 3. Solvatochromic data of **CZ_1** and **CZ_2**

Molecules	Parameters	Toluene	THF	DCM	DMF	Acetonitrile
	f (ε,n)	0.014	0.210	0.217	0.276	0.305
	ET (30) kcal.mol^{-1}	33.9	37.4	40.7	43.2	45.6
CZ_1	λ_{abs}[a] (nm)	424	425	426	428	429
	λ_{emi}[b](nm)	552	556	558	559	565
	Stokes shift (cm^{-1})	5468	5543	5553	5575	5610
CZ_2	λ_{abs}[a] (nm)	410	413	416	418	420
	λ_{emi}[b](nm)	520	526	532	538	542
	Stokes shift (cm^{-1})	5159	5273	5243	5336	5359

[a] Absorption spectra measured in various solvents (concentration of 10^{-5} M)

[b] Emission spectra measured in various solvents (concentration of 10^{-5} M)

Table 4. The electrochemical characterization data of **CZ_1** and **CZ_2**

Molecules	E_{OX} **(V *vs.* NHE)**	E^{a}_{OX} **(V *vs.* NHE)**[#]	E_{HOMO} **(eV)**[d]	E_{LUMO} **(eV)**[d]
CZ_1	0.67	–1.85	–5.37	–2.85
CZ_2	0.69	–1.89	–5.39	–2.81

The E* values were formulated by: $E_{OX}^{*} = E_{OX} - E_{0\text{-}0}$. [d] All the potentials were generated during CV investigations in 0.1 M Bu_4NPF_6 in DMF, with platinum electrode diameter: 1 mm, sweep rate: 100 mVs^{-1}

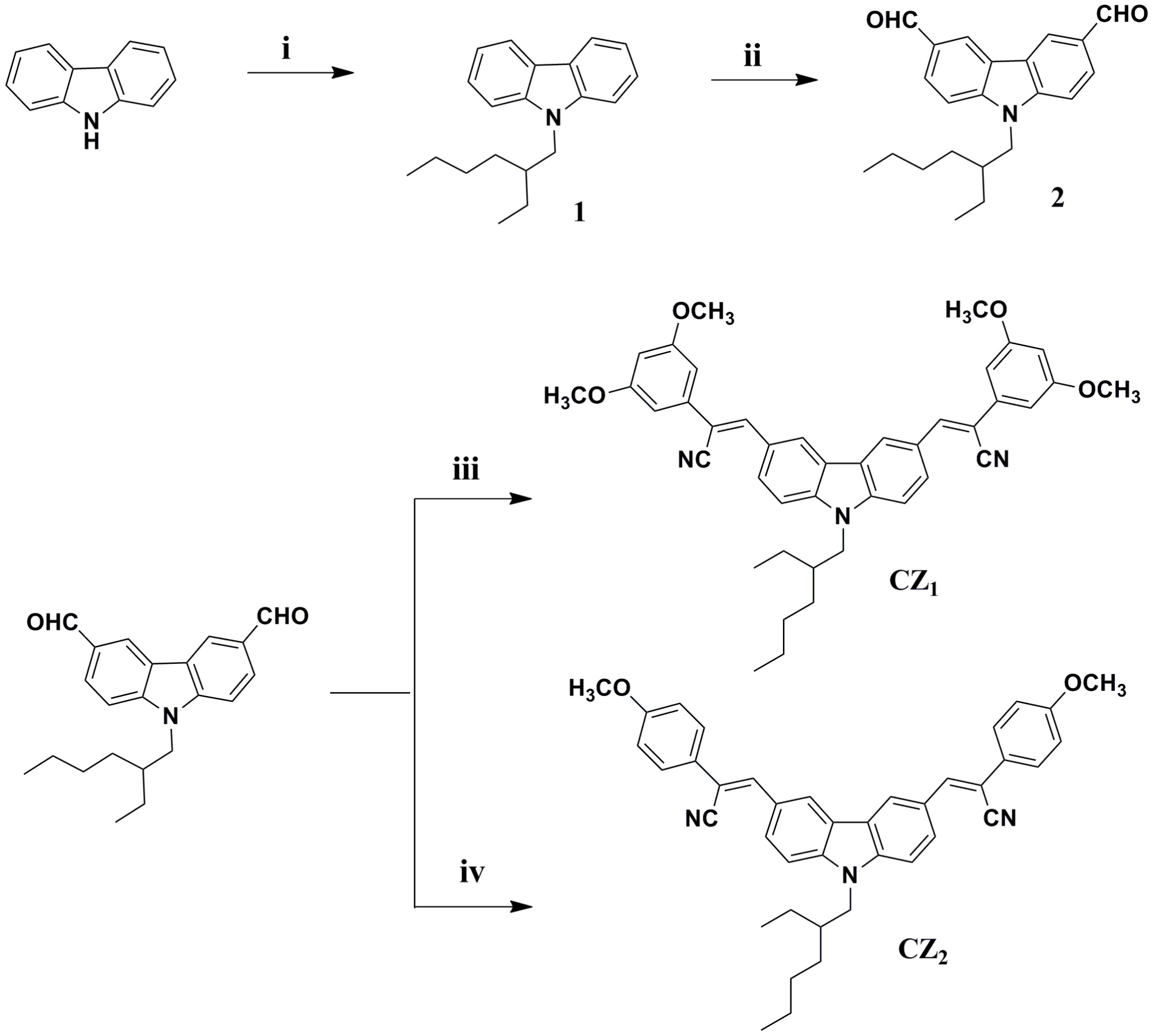
i
ii
iii
iv
1
2
CZ1
CZ2
OHC
CHO
OCH3
H3CO
NC
CN
N
H

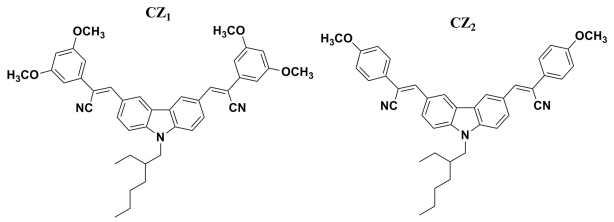

php_13337_f1.jpg

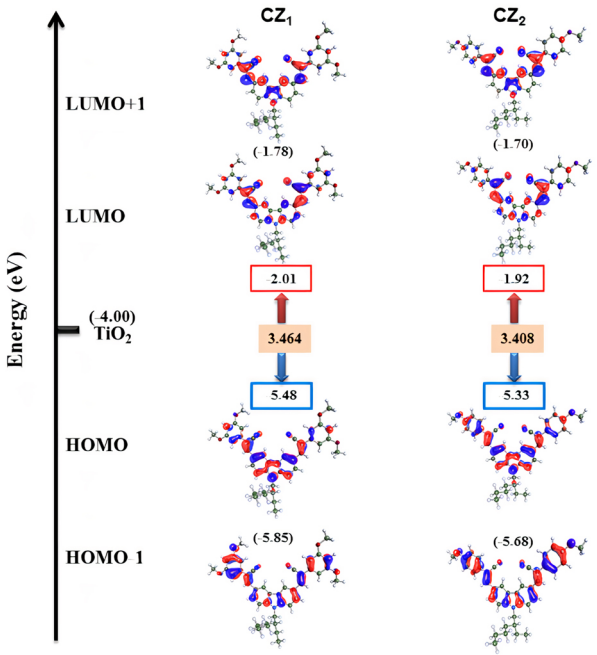

php_13337_f2.jpg

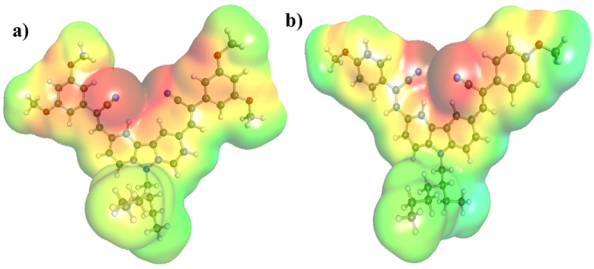

php_13337_f3.jpg

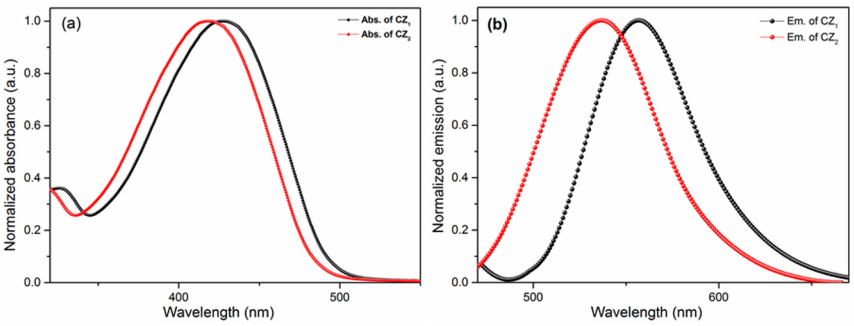

php_13337_f4.jpg

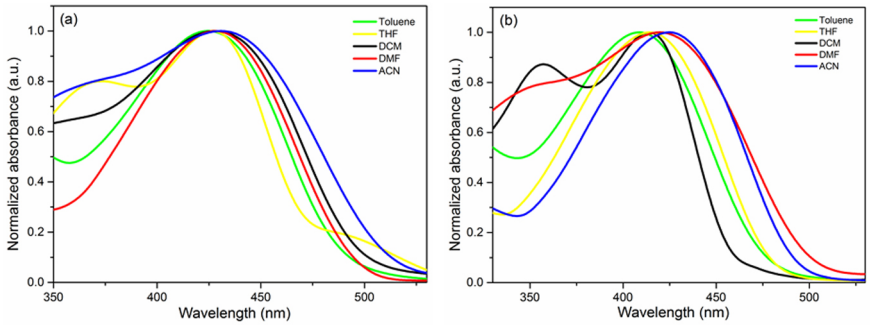

php_13337_f5.jpg

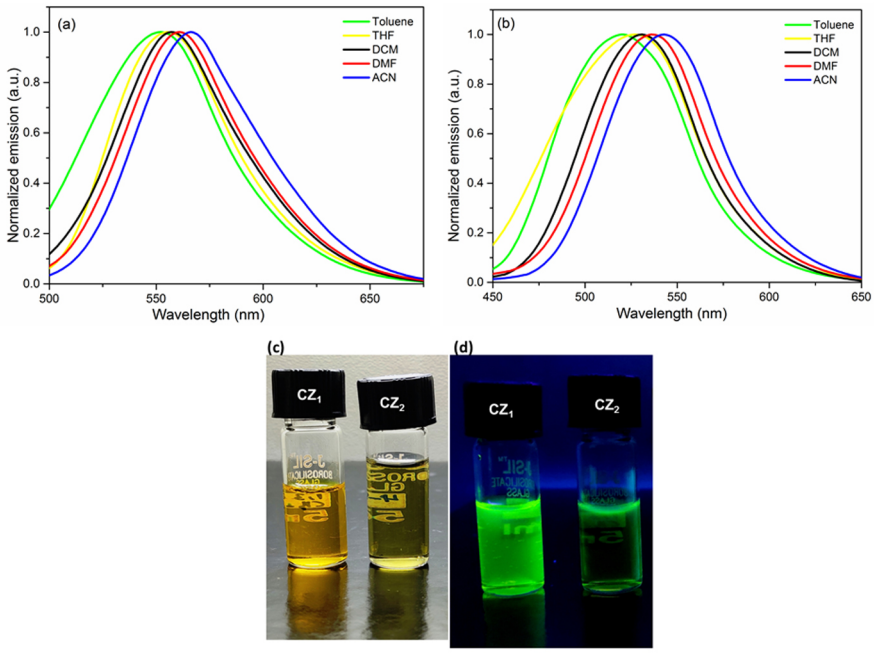

php_13337_f6.jpg

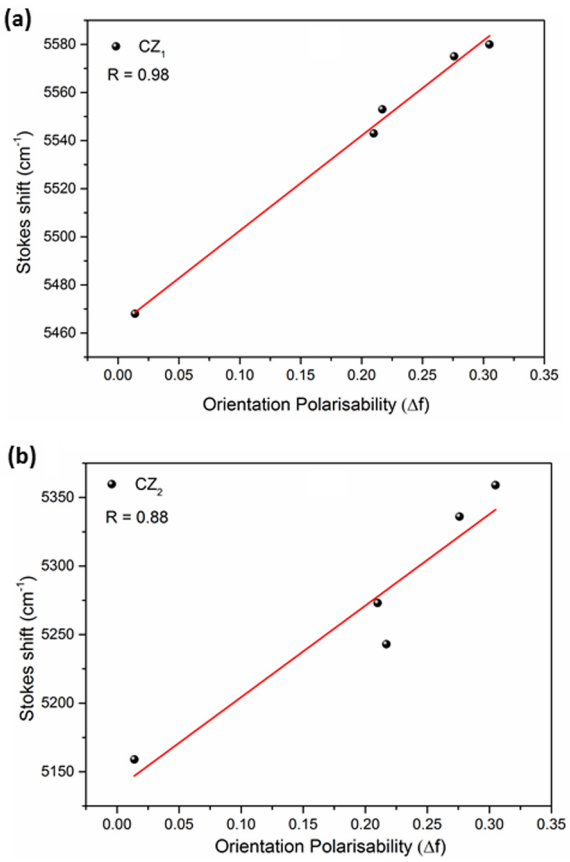

php_13337_f7.jpg

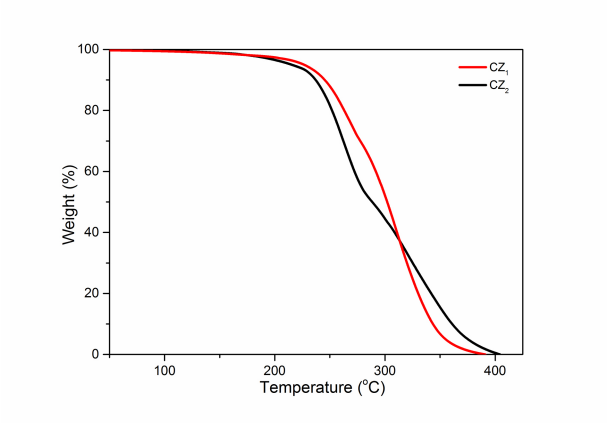

php_13337_f8.jpg

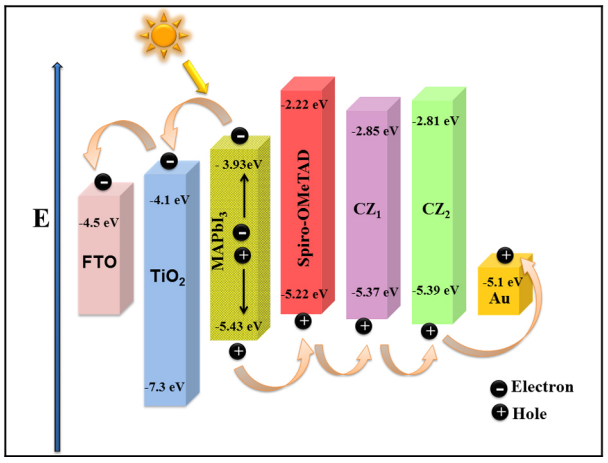

php_13337_f9.jpg